

## **1/3D MODELING OF THE CORE OF A PHWR NUCLEAR POWER PLANT**

**Santiago Corzo, Damian Ramajo and Norberto Nigro**

*Centro de Investigación de Métodos Computacionales CIMEC-UNL-CONICET, Colectora ruta 168, paraje el pozo (3000) Santa Fe, Argentina, santiagofcorzo@gmail.com*

**Keywords:** 1/3D modeling, PHWR, flow and thermal distribution

**Abstract.** A multi-dimensional CFD model to simulate the in-core coolant circuit of a Pressure Heavy Water Reactor (PHWR) of a nuclear power plant was performed. Three-dimensional (3D) detailed modeling of the upper and lower plenums, the downcomer and the hot-leg and cold-leg nozzles was linked with a finite volume one-dimensional (1D) one-phase code for modeling the behavior of all the 451 coolant channels. Suitable functions for introducing the distributed pressure drop (friction losses) and concentrated losses (spacer grids, inlet restrictors and outlet throttles) allowed to obtain the pressure variation along the channels. Moreover, the axial power distribution for each hydraulic zone was taken into account. Results were compared with the previously obtained with a zero-dimensional (0D) code getting more realistic temperature patterns at the upper plenum. Although the present model is one-phase, the prediction of the variation of pressure and temperature along the channels allow to a better identification of the location of incipient boiling by comparing with the local saturation temperature. This model is the previous step before perform a 1/3D two-phase model to evaluate in-channel subcooled boiling.

## 1 INTRODUCCION

The Nuclear Power Plant Atucha II (CNA II) has a pressurized heavy water reactor (PHWR) with an expected total thermal power of 2160 MWt and electric power of 745 MWe. The core has a vertical configuration of 451 cooling channels (CC) housed in the moderator tank. Each CC has the aim to remove the thermal power generated by fission of atoms through a coolant flow pumped under high pressure from the lower-plenum to the upper-plenum. The fuel bundle inside each CC is composed by a set of 37 fuel rods of 5.3 m active length with 13 spacers to strength the fuel assembly. The CC are arranged in a 272 mm trigonal lattice pitch within the moderator tank. CNA II will employ a fuel composed of natural and enriched uranium (0.85% of  $^{235}\text{U}$ ) and Deuterium heavy water ( $\text{D}_2\text{O}$ ) for cooling and moderation purposes.

The Reactor Pressure Vessel (RPV) of CAN II can be divided in the lower and the upper plenums, the downcomer, the moderator tank and the coolant channels. The coolant enters to the RPV through two cold legs and it downs to the lower plenum through the annular downcomer. A 3D draw of the coolant circuit is shown in [Figure 1](#). In each one of the two loops the hot coolant flows through the hot leg from the RPV to the steam generator to transfers the heat to the secondary circuit, then the cold coolant flows to the coolant pump to recover the high pressure and returns to the RPV through the cold leg.

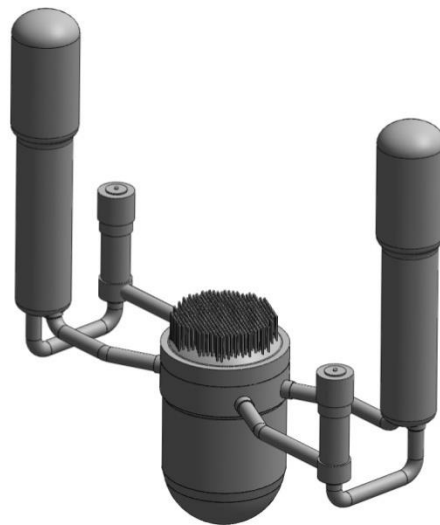


Figure 1: CNA II coolant circuit

Coolant enters to the CC through an inlet nozzle placed at the lower plenum. The nozzle can contains a flow restrictor for controlling the mass flow rate. Then coolant flow ups extracting heat from the 37 fuel rods and flow out through an outlet throttle at the upper plenum. The pressure drop along the CC is caused by concentrated form losses (sudden area change) at the inlet nozzle, the outlet throttle and the 13 spacers and by friction losses along the fuel rod and tube channel walls. The predicted pressure drop along the CC is 6 bar while the total pressure drop along the RPV circuit is around 7 bar.

The coolant is collected in the upper plenum which has a convex ellipsoidal shape housing 9 hafnium and 9 steel control rods. Moreover, the upper plenum is crossed by the 451 CC and the moderator collector output. All these components affect the velocity flow and thermal distribution in the upper-plenum. The coolant water follows to the steams generators by two hot-legs diametrically opposed. The secondary light water loop is boiling in the steam

generator and the heavy water leaves the boiler by the cold leg toward to the pumps. The fluid is pumped by the cold leg and enters in the RPV as shown in Figure 1.

Figure 2 at the left shows a cross section view cutting one hot-leg and one cold-leg of the RPV. Inside the RPV, the lower plenum has a flow distributor composed of rhomboidal cells housing the CC inlets. Each cell can groups until 9 CCs (see Figure 2 at the right). The coolant enters to the CCs and flow ups towards the upper plenum, extracting heat from the fuel bundles.

The scratched solids above the upper and below the lower plenums are the filler bodies, which serve to reduce the volume of the coolant in the reactor coolant system.

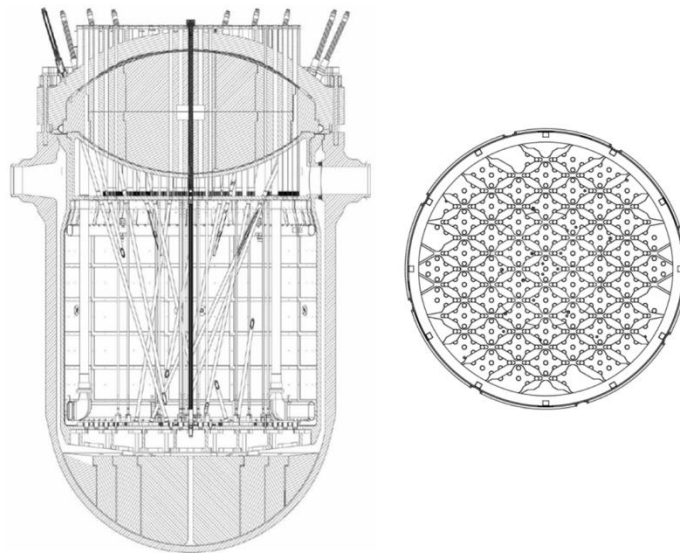


Figure 2: Left: cross sectional cut of the RPV. Right: sketch of the rhomboidal flow distributor at the lower plenum and the location of the CCs

The 451 CCs are grouped in 5 hydraulic zones (HZ) in which one of them the mass flow rate (MFR) is different attending to the radial power distribution of the reactor. This arrestment of different channel regime is produced by flow restrictors (except for the HZ 5 at the center of the RPV) placed at the CC inlets. Therefore the MFR is limited in each HZ. Figure 3 shows the HZ distribution. The HZ 5 is the most important, containing 253 of the 451 CCs and around 70% of the total coolant flow. The principal aim of the flow restrictions is to obtain an equilibrium between the heat released and the MFR in each CC.

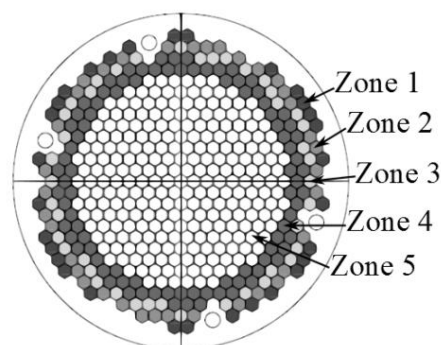


Figure 3: Location of the hydraulic zones

Due to the large dimensions of the RPV and the burn up and fuel efficiency, each fuel bundle trips during the fuel life period from the center of the reactor (at the beginning of life) to the periphery (at the end of life) until is removed from the reactor. This operation named refueling is continuously carried on while reactor is in operation. The refueling strategy along with the neutronic stratification because on the large core diameter (around 6 mts) causes the radial power distribution while the high core height induces the axial power one. The central CCs heated the coolant more than the periphery channels. Consequently, it is expected that coolant rises the highest temperatures at central CC. Tentative radial and axial power distributions were obtained for the five HZ from the Final Security Analysis Report (FSAR chapter IV, 2011). Table 1 summarizes the principal characteristics of the five HZ. Note that the channel power limit, and the corresponding MFR, increases almost three times from the HZ 1 to the HZ 5.

Property	Hydraulic zone				
	1	2	3	4	5
Total number of CC	30	36	42	90	253
Maximum channel power (MW)*	2.239	2.992	3.959	5.422	6.863
Minimum channel power (MW)*	1.908	2.640	3.641	5.442	6.343
Average channel power (MW)*	2.052	2.812	3.837	5.268	6.661
Channel power limit (MW)	2.524	3.158	4.036	5.565	7.062
Nominal MFR	9.29	11.70	15.08	21.27	27.73

\*Estimated by simulation (Courtesy of NASA)

Table 1: Characteristics of the 5 hydraulic zones

Several researchers has been studied the pressure drop in specific reactor components. The majority is devoted to characterize the fuel bundles (Le Corre et al, 2010; Vijayan et al, 1999; Anglart et al, 1997). Another authors discussed about the thermal distribution in Pressure Water Reactors (PWR) and void fraction production (Krepper et al, 2007; Kurul and Podowsky, 1991).

There are not many simulations that analyze the whole reactor without use 1D transients solvers like as Relap (Carlson et al, 1990), Athlet (Lerchl et al, 1995) or Cobra (Thurgood et al, 1983). These powerful software's give complete descriptions of the plant in nominal conditions as well as accident events. They allow the user to make simulations and analyze the response of the plant under accidents like LOCA (Loss of Cooling Accident) (Chen et al, 1994). On the other hand, Computational Fluid Dynamics (CFD) simulations of the RPV are limited by the number of degree of freedom. For this reason, a full CFD-3D model representing all CC would demands a huge mesh with high refinement around spacers and throttles. This model is impossible to carry out with the actual power computing. Consequently, we propose an approach coupling 3D domains of the upper plenum and the lower plenum with a suitable 1D code for CC modeling. The 1/3D coupling gives a complete description of the coolant circuit of the RPV, giving more detail where it is required. The present work is the second stage improving the original model in which the CC were modeled

by zero dimensional (0D) heat and momentum balance (Ramajo et al, 2011, Ramajo et al, 2013).

CNA II as well as CNA I are the only plants of its kind in the world. Any other similar nuclear power plant was constructed with this technology. Although the experience gained with CNA I, CNA II is two times larger than the first, getting a challenge, especially for CFD simulations. For this reason, the main objective of this study is to provide useful information about the thermo-hydraulic behavior in the RPV.

## 2 MATHEMATICAL FORMULATION

At the moment the 3D model is formulated as one-phase Newtonian flow with dynamic and thermo-physical properties computed for high pressure high temperature by the IAPWS-IF97 database (Wagner et al, 200). Steady state simulations were performed using the finite volume software ANSYS-CFX 13. 1D code was also formulated using finite volume method in fortran 90 and dialoging with CFX using the User Fortran Routine (UFR) tools. Compressible fluid was chosen attending to the variation of density as function of temperature and pressure.

### 2.1 3D formulation

The governing equations for the 3D model are described as follow:

$$\frac{\partial \rho}{\partial t} + \nabla \cdot (\rho U) = S_S \quad (1)$$

where  $\rho$  is the density,  $U$  the velocity and  $S_S$  is a source term used to put or remove mass from the 1D to 3D coupling. Regarding the momentum equation, it can be written as:

$$\frac{\partial(\rho U)}{\partial t} + \nabla \cdot (\rho U U) = -\nabla p + \nabla \cdot \bar{\tau} + \rho \bar{g} + S_M \quad (2)$$

where  $p$  is the static pressure,  $\bar{\tau}$  is the shear stress tensor and  $S_M$  is the momentum source introduced with the mass from the CC. The pressure-velocity coupling was solved using the SIMPLE algorithms (Rhie and Chow, 1983).

Energy balance is accomplished in terms of enthalpy by:

$$\frac{\partial(\rho h)}{\partial t} - \frac{\partial p}{\partial t} + \nabla \cdot (\rho U h) = \nabla \cdot (\kappa \nabla T) + \nabla \cdot (U \bar{\tau}) + S_E \quad (3)$$

Where  $h$  is the static enthalpy,  $\kappa$  is the thermal conductivity and  $S_E$  is the enthalpy of the mass which comes from the CC.

The standard two equation  $k$ - $\varepsilon$  model was employed to model turbulence and a standard logarithmic wall law was applied to represent the logarithmic velocity profile near walls, thus avoiding high mesh refinement (ANSYS-CFX Theory guide, 2010).  $k$ - $\varepsilon$  has been extensively employed to simulate multiphase systems due to its robustness and accuracy even with relatively rough meshes. The transport equations for the turbulent kinetic energy  $k$  and the turbulence dissipation rate  $\varepsilon$  are:

$$\frac{\partial(\rho k)}{\partial t} + \nabla \cdot (\rho U k) = \nabla \cdot \left( \frac{\mu_t}{\sigma_k} \nabla k \right) + G_t - \rho \varepsilon \quad (4)$$

$$\frac{\partial(\rho\varepsilon)}{\partial t} + \nabla \cdot (\rho U \varepsilon) = \nabla \left( \frac{\mu_t}{\sigma_\varepsilon} \nabla \varepsilon \right) + \frac{\varepsilon}{k} (C_1 G_t - C_2 \rho \varepsilon) \quad (5)$$

Where  $\mu_t$  is the turbulent viscosity, which is obtained from the eddy viscosity model,

$$\mu_t = \frac{C_\mu \rho k^2}{\varepsilon} \quad (6)$$

$C_1$ ,  $C_2$ ,  $\sigma_k$ ,  $\sigma_\varepsilon$  and  $C_\mu$  are model constants, being 1.44, 1.92, 1.0, 1.3 and 0.09, respectively.

In Eq. (4), (5) and (6),  $G_t$  is a turbulence production term estimated from the velocity gradient and the turbulent viscosity  $\mu_t$  as:

$$G_t = \frac{1}{2} \mu_t (\nabla U + (\nabla U)^T)^2 \quad (7)$$

Steady state simulations were performed with a pseudo-time step of  $5 \times 10^{-3}$  sec RMS residuals for mass and momentum were less than  $5 \times 10^{-4}$  while for energy and turbulence were less than  $5 \times 10^{-6}$  and  $1 \times 10^{-4}$  respectively. The mass unbalance between the lower inlet and the upper outlet was carefully kept below 1%. Equations were solved using local parallel computing facilities in one Intel(R) Core(TM) i7 CPU 950 3.07 GHz, 12 GB RAM.

## 2.2 1D formulation

For 1D formulation turbulence and Reynolds stresses ( $\nabla \cdot \bar{\tau}$ ) were neglected since only the component associated with axial diffusion is conserved. However, these effects are small compared with the axial convective flow of momentum ( $\nabla \cdot (\rho U U)$ ). The wall diffusivity effect and the form pressure losses were modeled using empirical correlations for the coefficient of the Darcy–Weisbach equation. Finally, the transport equations take the following form:

$$\frac{\partial \rho}{\partial t} + \nabla \cdot (\rho U) = 0 \quad (8)$$

$$\frac{\partial(\rho U)}{\partial t} + \nabla \cdot (\rho U U) = -\nabla p + S_f + S_{sp} + \rho \bar{g} \quad (9)$$

$$\frac{\partial(\rho h)}{\partial t} - \frac{\partial p}{\partial t} + \nabla \cdot (\rho U h) = \nabla \cdot (\kappa \nabla T) + S_{ps} \quad (10)$$

In Eq (9)  $S_f$  and  $S_{sp}$  represent the pressure drops by wall friction and by the spacers. The introduction of the local pressure drop from the flow restrictor and the outlet throttle in Eq. (9) was avoided due to convergence problems. In order to consider these losses and due to the fact that they are located at the inlet and the outlet of the CC, a dynamic boundary condition was implemented in order to modify the pressure imposed at the CC ends. That is reducing the pressure at the lower end of the CC (inlet flow) accounting for the restrictor pressure loss and reducing the pressure at the upper end of the CC (outlet flow) accounting for the throttle pressure loss.

In Eq (10)  $S_{ps}$  is the energy source to account for the fission heat transfer.

Density variation due to temperature and pressure changes along the CC length is significant. In consequence it was necessary to take into account this effect in the code. On the other hand, in normal operation slow temporal density variations are expected ( $\frac{\partial \rho}{\partial t} \approx 0$ )

allowing to use the density from the previous time step. Thus, temporal derivatives in Eq. (9) and (10) were discretized as:

$$\frac{\partial(\rho U)}{\partial t} \cong \frac{\rho^{n-1}}{dt} (U^n - U^{n-1}) \quad (11)$$

$$\frac{\partial(\rho h)}{\partial t} \cong \frac{\rho^{n-1}}{dt} (h^n - h^{n-1}) \quad (12)$$

The frictional pressure drop in Eq. (9) is computed by Darcy (Moskva et al, 1960):

$$S_f = \left(\frac{dp}{dx}\right)_f = \frac{1}{2} \frac{\rho}{D_h} C_f U^2 \quad (13)$$

Where  $D_h$  is the hydraulic diameter and  $C_f$  is the Darcy friction factor obtained by solving the modified Colebrook equation.

Similarly the spacer pressure drops are computed as:

$$S_{sp} = \left(\frac{dp}{dx}\right)_{sp} = \frac{1}{2} \frac{\rho}{dx} C_{sp} U^2 \quad (14)$$

In Eq. (14)  $C_{sp}$  is a form coefficient depending on the local Reynolds number. Correlations for predicting the pressure drop can be found in literature for typical spacer grids (Anglart et al, 1997; Brennen, 2005; Ghiaasiaan, 2008). In this work  $C_{sp}$  was obtained from CFD simulations previously achieved for the real spacer geometry and different flow conditions (Corzo et al, 2011). Both expressions (Eq. (13) and (14)) are non-linearly dependent on velocity in momentum equation. For that, the discretized form of these expressions would be quadratic in velocity and the resulting system of algebraic equations would therefore be non-linear. There are two possible solutions for this problem; either use a solver for non-linear systems, or linearize these terms (Ferziger et al, 1999). For example, the linearized form of Eq. (13) can be written in semi-implicit or explicit form:

$$S_f = \frac{1}{2} \frac{\rho}{D_h} C_f U^2 \approx \frac{1}{2} \frac{\rho}{D_h} C_f (U^{n-1} U^{n-1}) \approx \frac{1}{2} \frac{\rho}{D_h} C_f (U^{n-1} U^n) \quad (15)$$

Table 2 summarizes the form and skin coefficients used for each HZ. The outlet throttle coefficient  $C_{ot}$  was previously obtained by CFD (Corzo et al, 2011) while the inlet flow restrictor coefficient  $C_{ir}$  was obtained from experiments (FSAR chapter IV, 2011).

CC component	Pressure drop coefficient				
	1	2	3	4	5
Hydraulic zone					
Inlet flow restrictor ( $C_{ir}$ )	847.77	478.42	241.61	73.43	1.09
Outlet throttle ( $C_{ot}$ )	1.86	1.86	1.86	1.86	1.86
Spacers ( $C_{sp}$ )	14.25	8.55	4.89	1.99	1.14
Fuel rod + channel wall ( $C_f$ )	0.0184	0.0175	0.0166	0.0155	0.0147

Table 2: Pressure drop coefficients for the different CC components

A semi-implicit implementation was used in the present code. As above mentioned, the restrictor and outlet throttle losses were explicitly imposed by modify the boundary condition at the CC ends. For that, an expression similar to Eq (14) was implemented using form coefficient extracted from experiment data for the restrictor and from CFD for the outlet throttle. All form coefficients were computed using the previous time step information ( $t^{n-1}$ ).

The 1D semi-compressible equation system was solved using Volume Finite Method (VFM) (Versteeg et al, 2007) based on the discretization proposed by Jasak (Jasak et al, 1996). The PIMPLE algorithm (hybrid PISO/SIMPLE) was chosen for solving the pressure-velocity coupling. Standard PISO algorithm is not feasible for this kind of flows due to the stringent constraint on time step size imposed by PISO. For this purpose PIMPLE algorithm was implemented. This hybrid coupling has an improvement in convergence and stability than PISO. The problem was solved using 4 internal PIMPLE iterations and 3 external PIMPLE iterations. The energy equation was solved in a staggered form after the pressure and velocity were actualized. The fluid properties ( $\mu$ ,  $\rho$  and  $\kappa$ ) were actualized at the beginning of each external PIMPLE loop.

### 3 COMPUTATIONAL MODEL

In the upper plenum, the hot legs, the 20 control and measurement rods, the 4 vertical moderator inlets and the 2 elbow moderator outlets were included. Moreover, a vertical cylinder was placed above each SSP to represent the extreme of the fuel assembly containing the mechanical coupling system for the refueling operation. As for the lower plenum, the cold legs, the downcomer and the rhomboidal flow distributor were included. The 3D domain was made from the assembly of two isolated domains; the upper domain and the lower one, which are joined through the SSPs which transport mass from one domain to the other.

The coupling between the 1D and the 3D domains was implemented in CFX using a novel strategy of sink/source points (SSPs) developed and assessed for the 0/3D previous model (Ramajo et al, 2013). The lower end (that is the inlet under normal flow condition) of each CC is represented by a SSP located at the 3D lower plenum domain. Similarly, the upper end of this CC is represented by a SSP located at the 3D upper plenum domain. Through these two points, the sink/source of mass  $S_S$  and momentum  $S_M$  and energy  $S_E$  in Eq. (1), (2) and (3) are modeled. The coupling was implemented using an UFR, which receives the current flow conditions (pressure and temperature) of the upper and lower SSPs of each CC, calculates the requested variables (MFR, Temperature and vertical velocity) and return the result at the beginning of each iteration of the 3D model. Figure 4 at the left shows a sketch of the coolant flow and the location of the two SSPs corresponding to one CC. Figure 4 at the right shows the 451 source points located in the upper plenum.

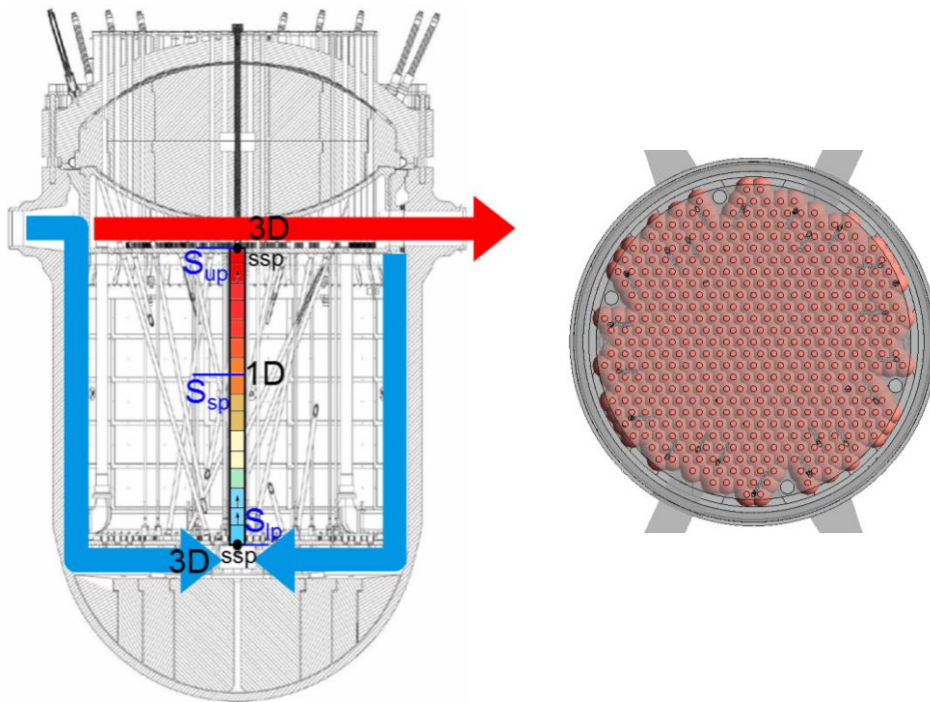


Figure 4: Left: 1/3D couple scheme. Right: SSPs in the upper plenum

Figure 5 shows schematically the model algorithm and the interaction between both domains. The coupling was explicit in terms of pressure and temperature. That means the 1D code computes the CCs transport variables using the previous time step state ( $p_l^{n-1}$ ,  $p_u^{n-1}$ ,  $T_l^{n-1}$ ,  $T_u^{n-1}$ ). Then, the 3D model updates the variables MFR, U, and T received from the UFR and solve the 3D field.

The heat transferred from the fuel rods to the coolant was included taking into account both the axial and radial power distribution at normal operation. Although coolant is heavy water, this preliminary work was performed with light water.

The 3D assembly domain was meshed with 9.128.118 cells (8.819.511 tetrahedrons, 3.302 pyramids and 305.305 wedges). The lower domain was composed by the cold legs, the downcomer and the lower plenum has a volume of 56.22 m<sup>3</sup>, containing 3.934.401 elements. On the other hand, the upper domain was composed by the hot legs and the upper plenum with a volume of 31.06 m<sup>3</sup> was discretized with 5.193.717 elements. As regards the 1D domain of each CC, it was meshed with 13 cells.

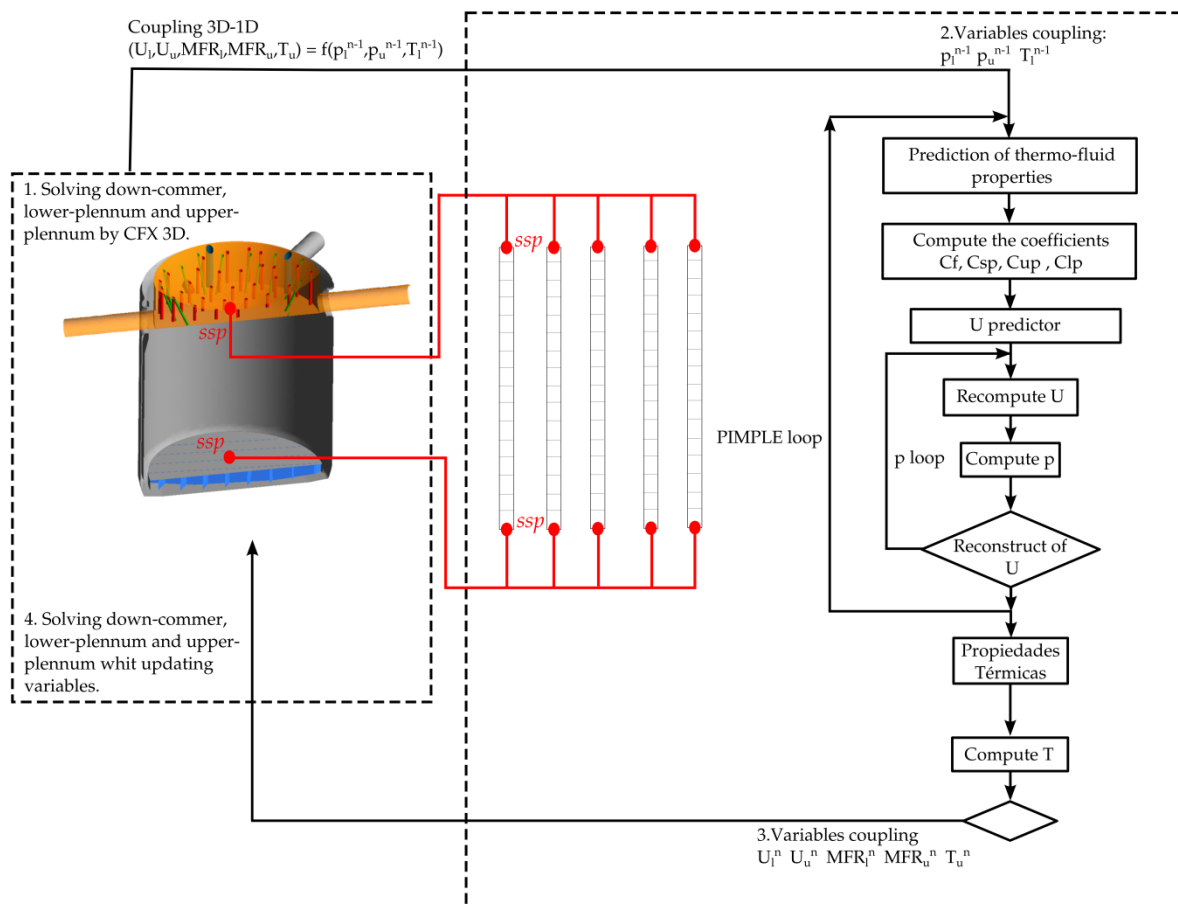


Figure 5: Model algorithm

#### 4 RESULTS AND DISCUSSION

Numerical results of the non-isothermal steady state solutions describing the overall flow behavior in the RPV are presented in this section. Those preliminary results allow to evaluate the potentiality of the developed computational model using SSPs and the 1D modeling and the pseudo-compressible formulation. Results allow estimate features such as the MFR in each HZ for comparing with the plant design data and the measurements performed until the plant startup. Moreover, the visualization of thermal distribution in the upper plenum and thermal stratification in the hot legs will be compared with temperature measurements once the plant rise nominal operation conditions.

The inlet and outlet pressure from the 3D model defines the nominal MFR in each CC according with its own pressure drop coefficients. But, these coefficients depend on the MFR. In present research, solving the 1D domain in each 3D iteration brings convergence problems in the 3D solver. For this reason, the 1D calculus was done every 35 iterations of the 3D model. This can occur due to the fact that the SSP interaction domains is a dynamic boundary condition in a steady state 3D model simulation.

Figure 6 shows the transport variables fields along one CC of each HZs. Velocity increases along the channel due to density reduction caused by temperature increment and pressure reduction. The pressure drop caused by the inlet restrictors dominates over the rest losses in HZ 1, 2, 3 and 4. A local high pressure drop occurs at the inlet of the CC (except for HZ 5 due to the absence of flow restrictors). After that pressure continues decreasing due to frictional

losses at the walls and form losses at the spacers. Excepting for the unthrottled zone (HZ 5), the largest pressure drop are caused for the presence of the flow restrictors.

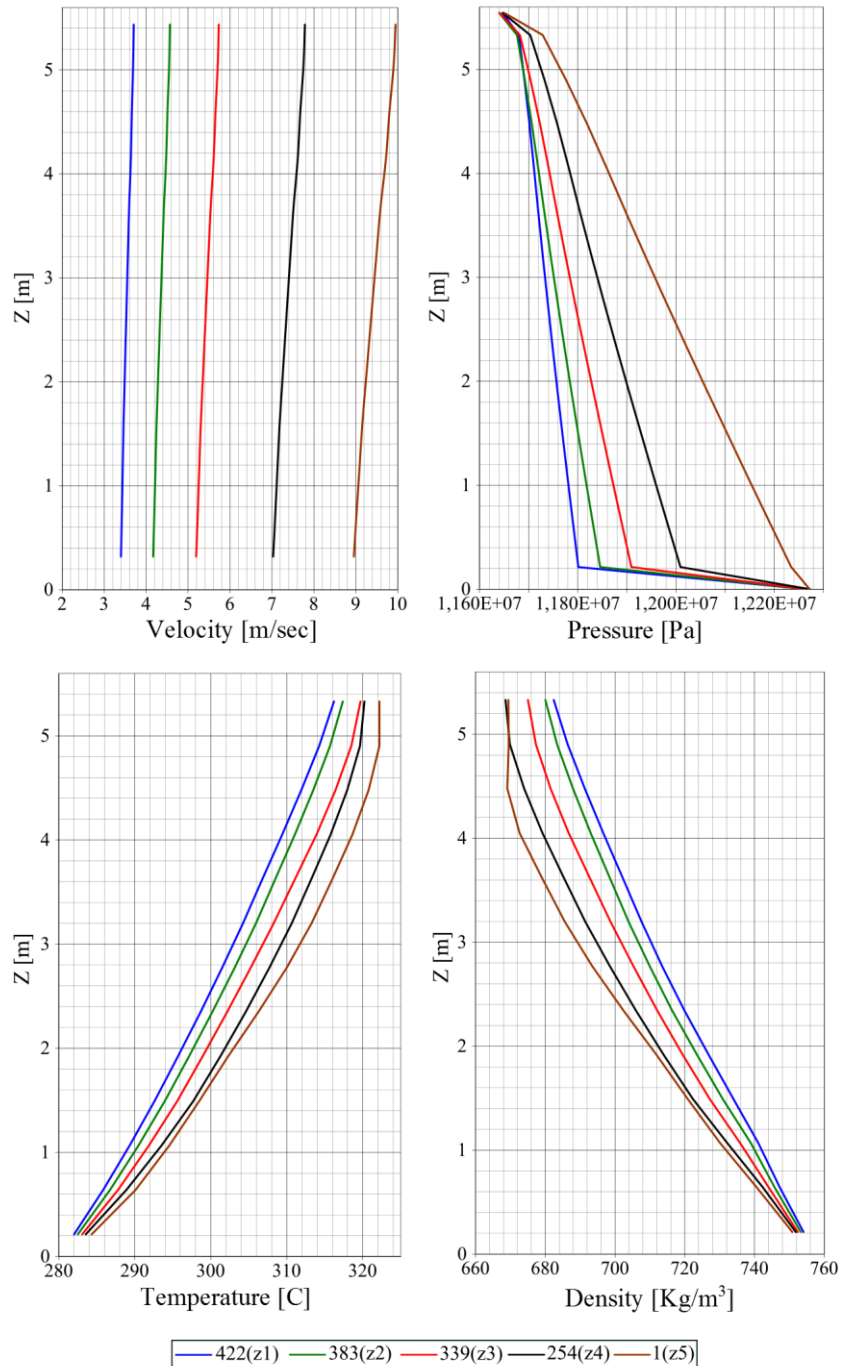


Figure 6: 1D solutions for CC: 1, 254, 339, 383 and 422 corresponding to different HZ. Left-up: velocity. Right-up: pressure. Left-down: temperature. Right-down: density

The local pressure at each control volume is used to calculate saturation temperature. Results show that coolant rises saturation for CC grouped in HZ 4 and 5. That takes place around 0.5 mts until the CC upper ends and after that saturation temperature is set for the coolant. The current implementation of the 1D code is one-phase. In consequence steam formation cannot be estimated.

Figure 7 shows the velocity pattern over a vertical plane cutting the cold legs. Although the joint between the cold legs and the downcomer have a divergent shape the flow detaches from the inner wall impacting the moderator tank wall and descending close to it. The flow inside the upper plenum is very complex. Inside the downcomer annulus the flow is not completely homogeneous and the velocity ranges from 1 to 5 m/s.

Inside the lower plenum all the rhomboidal cells of the distributor show vortex structures of the size of the cells. Velocities are quite higher at the central SSPs rising velocities up to 2 m/s.

Inside the upper plenum the maximum values of velocity are achieved in central channels. For visualization reasons the cylinders above the SSPs were not lighted in Figure 7.

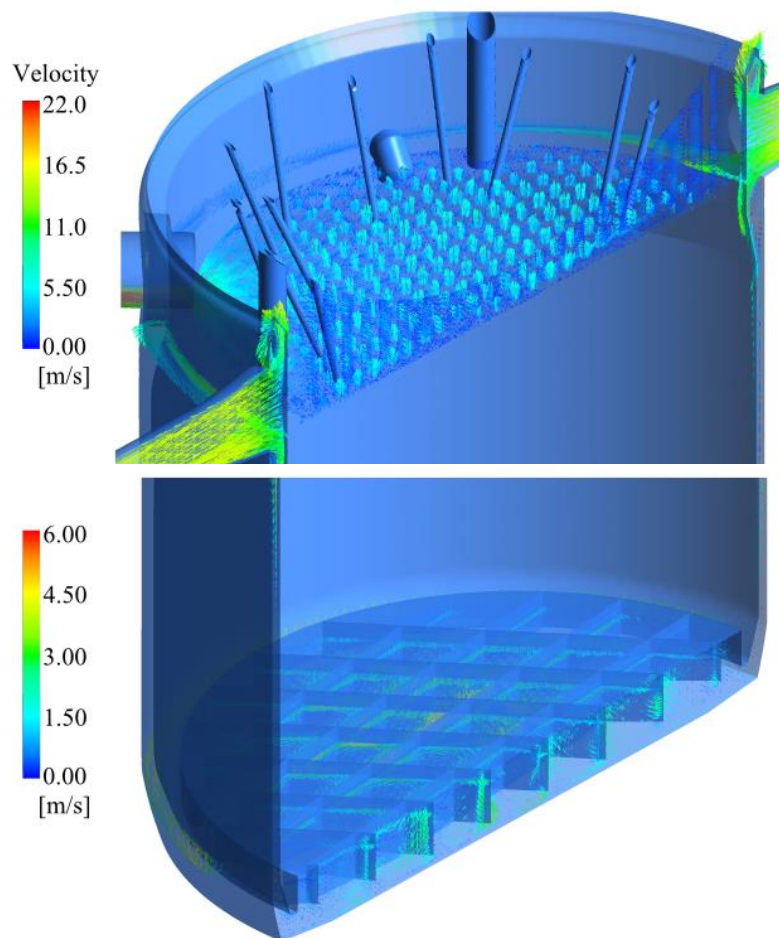


Figure 7: Velocity pattern over some cutting planes

Figure 8 allows to visualize the velocity and the temperature pattern over a vertical plane cutting the hot legs. Note that flow is strong accelerated around the hot legs. Mixing is very intense in part due to the control rods and cylinders above the SSPs but mainly due to the velocity of the flow coming from the SSPs. The inlet and outlet moderator tank duct has not a significant effect on the flow. This could be because the strongly coolant agitation is located at the upper plenum core. It is important to see the thermal stratification between the top and the bottom zones inside the upper plenum. This effect was studied by some authors (Shen et al, 2002) and it also persist along the hot legs as showed in the cross sectional cut planes in Figure 9 in which temperature difference can rises 2°C.

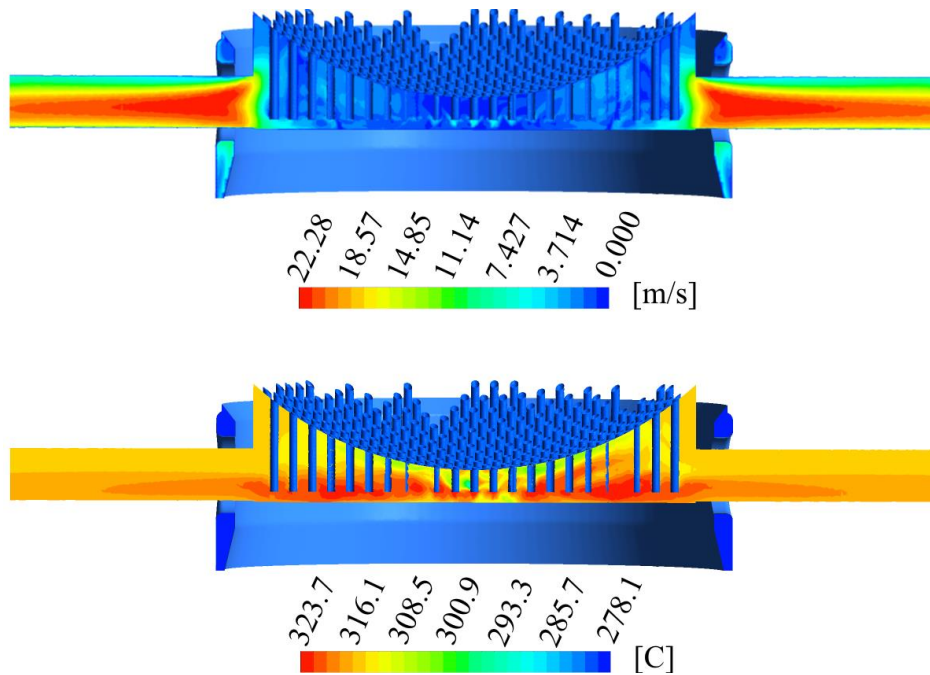


Figure 8: Velocity and Temperature profile over a vertical plane cutting the hot legs

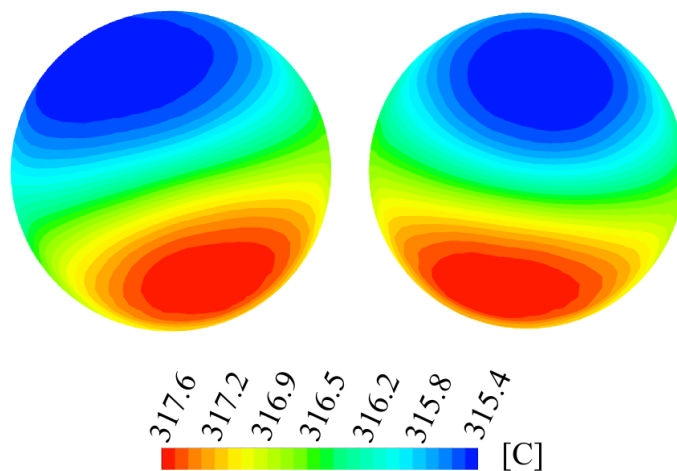


Figure 9: Temperature pattern at the hot leg outlets

Figure 10 shows the temperature profile over a horizontal plane located at the same height of the upper SSPs. Note the thermal distribution corresponding to the power discretization in the HZ. The periphery of the upper plenum holds temperatures under saturation while coolant from CCs of HZ 4 and HZ 5 rises saturation. However, a strange behavior occurs in the central zone where a spot of low temperature take place. Although the over-heating in some CCs, the average hot-leg temperature is holds under saturated conditions. This is explained by the strong mixing in the upper plenum.

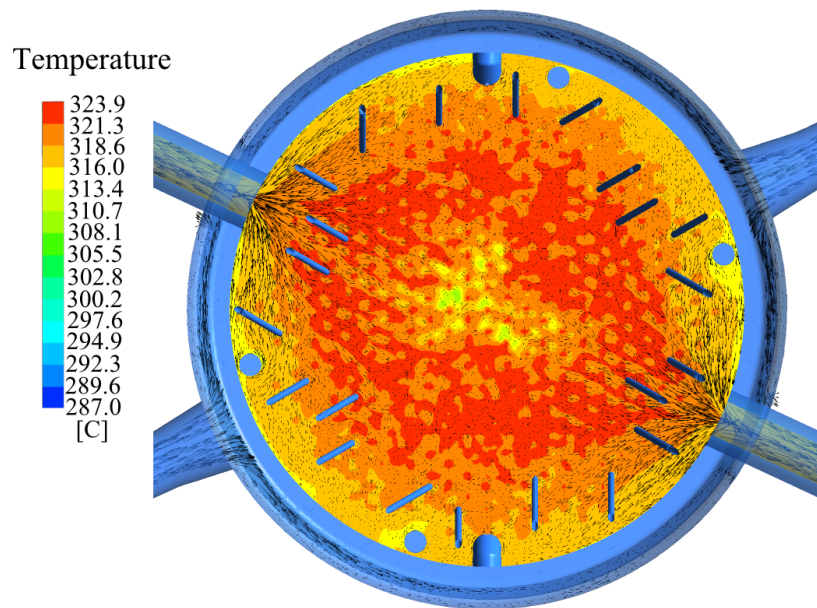


Figure 10: Temperature pattern over a horizontal plane cutting the upper plenum

## CONCLUSIONS

In view of the results presented above we conclude that the model developed is in good agreement with the design data of the plant. Although the one-phase limitations the present work gives useful information about the coolant flow in the RPV. Results are precursors by the fact that the strategy of using SSPs opens the possibility of modeling the overall RPV, which will be impossible without the implementation of a simplified model for the CCs. This kind of strategy had not been reported in the open literature yet.

The obtained results allowed to verify the smaller pressure drop expected at the downcomer. The behavior of the flow distributor at the lower plenum showed to be in agreement with the expected, that evidenced by the small variation on the static pressure at the lower points of the SSPs. The 1/3D coupling allowed estimating the pressure drop and thermal distribution in the 451 channel. The semi-compressible formulation gave us a good approach of the density variation and its effect over the momentum quantities in steady state solutions.

The mixing in the upper plenum induced by the complex geometry was noted. Temperature distribution is strongly affected by this effect. The transversal temperature gradients typically expected in the hot legs has been observed. Results provided from these simulations are very helpful due to the lack of information about this kind of nuclear power plants.

The 1D code for modeling the CCs showed more realistic predictions than the previous 0D code. Moreover, the one-phase model seems to be useful to identify the overheating zones. Future work is oriented to implementation of a two-phase model to approach the sub-cooled boiling in channels.

## GLOSSARY

CNA:	Central Nuclear Atucha.
PHWR:	Pressurized Heavy Water Reactor.
CC:	Coolant Channel.

HZ:	Hydraulic zone.
RPV:	Reactor Pressure Vessel.
MFR:	Mass Flow Rate.
CFD:	Computational Fluid Dynamics.
LOCA:	Loss of Cooling Accident.
SSP:	Sink/Source Point.
PISO:	Pressure Implicit with Split Operator
SIMPLE:	Semi-Implicit Method for Pressure-Linked Equations
PIMPLE:	Hybrid PISO/SIMPLE algorithm.
VFM:	Volume Finite Method.
UFR:	User Fortran Routine.
U:	Velocity.
p:	Pressure.
T:	Temperature.
$\rho$ :	Density.
g:	Gravity acceleration.
h:	Enthalpy.
$\bar{\tau}$ :	Stress tensor.
$\mu$ :	Dynamic Viscosity.
$\kappa$ :	Thermal Conductivity.
$S_S$ :	Mass Sink/Source.
$S_M$ :	Momentum Sink/Source.
$S_E$ :	Energy Sink/Source.
k:	Turbulent kinetic energy.
$\varepsilon$ :	Turbulence dissipation rate.
$\mu_t$ :	Turbulent viscosity.
$G_t$ :	Turbulence production.
$S_f$ :	Pressure drop by wall friction.
$S_{sp}$ :	Pressure drop by the channel spacers.
$S_{up}$ :	Pressure drop by throttle.
$S_{lp}$ :	Pressure drop by inlet restrictors.
$S_{ps}$ :	Power source.
$D_h$ :	Hydraulic diameter.

## ACKNOWLEDGEMENTS

Authors want to thanks to Universidad Nacional del Litoral (CAI+D 2011 PJ 500 201101 00015 and CAI+D PI 501 201101 00435) and CONICET (PIP 112 201101 00331). Also they want to thanks to Autoridad Regulatoria Nuclear (ARN) for their financial support.

## REFERENCES

- ANSYS-CFX solver theory guide, 2010.
- Anglart H., Nylund O. Kurul N., Podowski M.Z., CFD prediction of flow and phasedistribution in fuel assemblies with spacers, *Nuclear Eng. and Design*, 177:215-228, 1997.

- Brennen C., *Fundamentals of Multiphase Flows*, Cambridge Univ. Press, 2005.
- Carlson, K., Riemke, R., Rouhani, S., Shumway, R., and Weaver, W., *Relap5/mod3code manual, volume i: code structure, system models and solution methods*. INEL Report, NUREG/CR-5535 (EGG-2596), 1990.
- Chen, NCJ, Wendel, Mark W, Yoder and Graydon L, Conceptual design loss-of-coolant accident analysis for the advanced neutron source reactor, *Nuclear technology*, 105, 1, 104-122, American Nuclear Society, 1994.
- Corzo S., Ramajo D., Marquéz Damian S. and Nigro N., CFD Simulation inside a PHWR Coolant Channel of the Atucha II Nuclear Power Plant, *ENIEF 2011*, Noviembre de 2011, Rosario, Argentina, 2011.
- Ferziger J. and Peric M. *Comp. methods for fluid dynamics*, volume 3. Springer Berlin, 1999.
- FSAR chapter IV, NASA, 2011.
- Ghiaasiaan M., *Two-Phase Flow, Boiling and Condensation*, Cambridge Univ. Press, 2008
- Jasak H. Error analysis and estimation for the finite volume method with applications to fluid flows. *Direct*, 1000(June), 1996.
- Krepper E., Koncar B., Egorov Y., CFD modeling of subcooled boiling-Concept, validation and application to fuel assembly design, *Nuclear Eng. and Design*, 237:716-731, 2007.
- Kurul N., Podowsky M., On the modeling of multidimensional effects in boiling channels, *ANS Proc. 27th National Heat Transfer Conference*, Minneapolis, MN, 28-31, 1991.
- Le Corre J.M., Yao S.C, Amon C., A mechanistic model of critical heat flux under subcooled flow boiling conditions for application to one-and three-dimensional computer codes, *Nuclear Eng. and Design*, 240:235-244, 2010.
- Lerchl, G., and Austregesilo, H., The athlet code documentation package. Users Manual, GRS-P, 1, 1995.
- Moskva, Leningrad, Handbook of Hydraulic Resistance. Goudarstv ennoe Energetic heskoeIzdatel'stvo, 1960.
- Ramajo D., Corzo S., Schiliuk N. and Nigro N., 3D modeling of the primary circuit in the reactor pressure vessel of a PHWR, *Nuclear Eng. and Design*, in press, 2013.
- Ramajo D., Corzo S., Marquéz Damian S. and Nigro N., Computational fluid dynamics simulation of the Atucha II nuclear power plant reactor, *ENIEF 2011*, Noviembre de 2011, Rosario, Argentina, 2011.
- Shen, X., Yu, P and Yang, G, Hydromechanical investigation on 3 PWR upper plenum core structures, *Nuclear Eng. and Design*, 217, 1, 103-110, Elsevier, 2002.
- Thurgood, M., 1983. COBRA/TRAC, a Thermal-hydraulics Code for Transient Analysis of Nuclear Reactor Vessels and Primary Coolant Systems. The Commission.
- Versteeg H. and Malalasekera W. An introduction to computational fluid dynamics: the finite volume method. Prentice Hall, 2007.
- Vijayan P.K., Pilkhwal D.S., Saha D., Venkat Raj V., Experimental studies on the pressuredrop across the various components of a PHWR fuel channel, *Exp. Thermal and Fluid Science*, 20:34-44, 1999.
- Wagner W. and Cooper JR. The IAPWS industrial formulation 1997 for the thermodynamic properties of water and steam, *Journal of Engineering for Gas Turbines and Power*, 122(1)150:182, 2000.